Ferromagnetic 1H-$LaBr_2$ monolayer: a promising 2D piezoelectric

Mohammad Noor-A-Alam and Michael Nolan
Tyndall National Institute, Cork, Ireland

The discovery of two dimensional (2D) materials that have excellent piezoelectric response along with intrinsic magnetism is promising for nanoscale multifunctional piezoelectric or spintronic devices. Piezoelectricity requires non-centrosymmetric structures with an electric band-gap, whereas magnetism demands broken time-reversal symmetry. Most of the well-known 2D piezoelectric materials – e.g., 1H-MoS_2 monolayer – are not magnetic. Being intrinsically magnetic, semiconducting 1H-$LaBr_2$and 1H-VS_2 monolayers can combine magnetism and piezoelectricity. We compare piezoelectric properties of 1H-MoS_2, 1H-VS_2 and 1H-$LaBr_2$ using density functional theory. Our results show that ferromagnetic 1H-$LaBr_2$ 2D monolayer displays a larger piezoelectric strain co-efficient (d_{11}= -4.527 pm/V, which is close to d_{11}= 4.104 pm/V of 1H-VS_2 monolayer) compared to that of well-known 1H-MoS_2 monolayer (d_{11}= 3.706 pm/V), while 1H-MoS_2 monolayer has a larger piezoelectric stress co-efficient (e_{11}= 370.675 pC/m) than the 1H-$LaBr_2$ monolayer (e_{11}= -94.175 pC/m, which is also lower than e_{11}= 298.100 pC/m of 1H-VS_2 monolayer). These in-plane piezoelectric d_{11} coefficients are quite comparable with piezo-response of bulk wurtzite nitrides – e.g., d_{33} of GaN is about 3.1 pm/V. The large d_{11} for 1H-$LaBr_2$ monolayer originates from the low elastic constants, C_{11}= 30.338 N/m and C_{12} = 9.534 N/m. Interestingly, the sign of the piezoelectric co-coefficients for 1H-$LaBr_2$ monolayer is different to that of the 1H-MoS_2 or 1H-VS_2 monolayers. The negative sign arises from the negative ionic contribution of e_{11}, which dominates in the 1H-$LaBr_2$ monolayer, whereas the electronic part of e_{11} dominates in 1H-MoS_2 and 1H-VS_2. Furthermore, we explain the origin of this large ionic contribution of e_{11} for 1H-$LaBr_2$ in terms of the Born effective charges (Z_{11}) and the sensitivity of the atomic positions to the strain ($\frac{du}{d\eta}$). Surprisingly, we observe a sign reversal in the Z_{11} of Mo and S compared to the nominal oxidation states, which makes both the electronic and ionic parts of e_{11} positive, and results in the high value of e_{11}. Additionally, our interatomic bond analysis using crystal orbital Hamilton populations indicates that the weaker covalent bond in 1H-$LaBr_2$ monolayer is responsible for large $\frac{du}{d\eta}$ and elastic softening (lower elastic constants).

I. INTRODUCTION

Piezoelectric materials are used in wide range of important devices such as microphones, medical imaging, and sensors[1, 2]. Recently it has been demonstrated that the piezopotential originating from piezoelectricity can be used as a gate voltage to control the electronic band gap of a piezoelectric semiconductor, opening a new field of research named piezotronics[1, 2]. In this regard, 2D semiconductors are promising materials as they can sustain a large deformation[1, 2]. Moreover, these 2D materials show unique optical properties, for example valleytronics[3, 4]. Hence, 2D materials can be ideal for piezo-photonics where charges stemming from the piezoelectric effect can couple with light to significantly modulate the charge-carrier generation, separation, transport, and/or recombination in semiconducting nano-structures, promising better LED, photodetector, and solar cell[1, 2].

Piezoelectricity and valleytronics require broken inversion symmetry and a band gap. Promisingly there already exists a wide range of non-centrosymmetric and intrinsically piezoelectric 2D materials [3, 4]. On the other hand, there are only a few 2D semiconductors/insulators to date in which both time-reversal and inversion symmetry are broekn. Very recently, the co-existence of magnetism and piezoelectricity has been predicted in vanadium dichalcogenide monolayers[5]. However, how the magnetic ordering impacts on their piezoelectricity remains unexplored. This understanding will allow us to couple magnetism and piezoelectricity for realizing multifunctional piezoelectric devices.

A piezoelectric stress co-efficient (e_{ij}) – is defined as $\frac{\partial P_i}{\partial \eta_j}$,where ∂P_i is the induced polarization along i-direction in response to strain $\partial \eta_j$along j-direction) – can be split into two contributions – ionic part e_{ij}^{ion}, where ions are allowed to move under an applied strain and electronic part (also known as clamped-ion part) e_{ij}^{elc}, where ions are clamped under an strain. In many bulk materials, including wurtzite nitrides[6, 7], e_{ij}^{elc} is negative but is dominated by e_{ij}^{ion}, thus resulting in a positive value of e_{ij}. Generally, a positive longitudinal piezoelectric coefficient is expected as a tensile strain is expected to increase the induced electric polarization. However, very recently an anomalous negative piezoelectric co-efficient has been observed in the layered ferroelectric $CuInP_2S_6$ [6], which is explained in terms of its large negative e_{ij}^{elc} that is not overcome by positive e_{ij}^{ion}. Also, negative piezoelectric coefficients – due to their large negative e_{ij}^{elc} – have been observed in several hexagonal ABC ferroelectrics[8]. This raises an interesting question: can a negative total e_{ij} be obtained due to large negative e_{ij}^{ion}? To answer this question, we investigate three intrinsically piezoelectric monolayers, 1H-MoS_2, 1H-VS_2 and 1H-$LaBr_2$ and we discover 1H-$LaBr_2$ as a new 2D piezoelectric monolayer that has a negative piezoelectric co-efficient originating from a large negative e_{ij}^{ion}. Being a magnetic, semiconducting electride 1H-$LaBr_2$ is a unique monolayer, although it

has not been achieved experimentally yet, however, it is predicted to be feasible via chemical exfoliation from its layered bulk structure[9]. It combines peculiar features – for example, its electron density shows neither complete localization at an atomic site nor metal-like delocalization, rather occupies at the center of the hexagon that originates localized magnetic moments[10, 11]. Very recently, it has been predicted that this magnetism can be utilized for valley polarization[9]. However, its piezoelectric properties have been not been investigated to date.

Recently a number of 2D materials in the 1H structure (D_{3h} symmetry) have been predicted to show large piezoelectric co-coefficients [12–15]. These 2D materials still remains at the stage of fundamental research, understanding the origin of piezoelectricity can promote discovery of more 2D piezoelectrics. Encouragingly, piezoelectricity has also been experimentally confirmed in 1H-MoS_2 monolayer[16], and the value e_{11} (2.9x10^{-10} C/m) is in good agreement with first-principles calculations, e_{11}= 3.64x10^{-10}C/m[17]. Recently, coexistence of magnetism and piezoelectricity has also been predicted in 1H-VS_2 monolayer[5], although the coupling between magnetic order and piezoelectricity was not discussed. Note that research on these 1H structured 2D piezoelectrics is mainly devoted to find large piezoelectric coefficients, overlooking their sign as they generally show positive in-plane piezoelectric coefficients[5, 12–15, 17]. However, the origin of the piezoelectric co-coefficients in both magnitude and sign still remains unclear. Questions include: why is the e_{11} of 1H-MoS_2 monolayer larger than that of 1H-VS_2 monolayer? Why is the sign of the ionic part of e_{11} in 1H-MoS_2 monolayer positive, but negative in 1H-VS_2 monolayer? In this paper, we show that the answers to these questions have their origin in the Born Effective Charges (BECs), the sensitivity of the atomic positions in response to a strain ($\frac{du}{d\eta}$), and the bond strength. We also demonstrate that the 1H-$LaBr_2$ monolayer[9–11] can be a magnetic, piezoelectric material. Moreover, we show that antiferromagnetic ordering makes the isotropic piezoelectricity of ferromagnetic 1H-$LaBr_2$ monolayer anisotropic (i.e., $e_{11} \neq -e_{12}$).

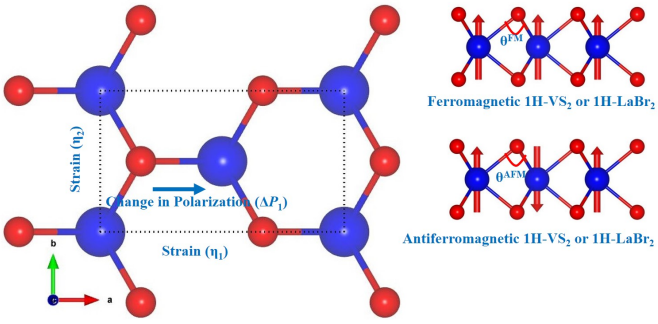

Figure 1. A rectangular unit cell; Blue and red balls represent Mo/V/La and S/O, respectively. The red arrow represents up or down spin state of an atom.

II. COMPUTATIONAL DETAILS

Our first-principles calculations are performed in the framework of spin-polarized density functional theory using projector augmented wave (PAW) potentials to describe the core electrons and the generalized gradient approximation (GGA) of Perdew, Burke, and Ernzernhof (PBE) for exchange and correlation as implemented in the Vienna Ab initio Simulation Package (VASP) [18–20] based on a plane-wave basis set. The valence electron configurations for La, V, Mo, S, Br are $4p^6\ 5s^2\ 6d^1$ (9 electrons), $3p^6\ 3d^4\ 4s^1$ (11 electrons), $4p^6\ 4d^5\ 5s^1$ (12 electrons), $3s^2\ 3p^4$ (6 electrons), $4s^2\ 4p^5$ (7 electrons), respectively. A cutoff energy of 500 eV for the plane-wave expansion is used in all calculations and all structures are fully relaxed until the Hellmann-Feynman forces on all the atoms are less than 10^{-3} eV/Å. An effective on-site coulomb interaction parameter (U_{eff}) of 6.5 eV is used for the La f-electrons[10]. The lattice parameters and internal coordinates of the 2D structures are fully relaxed to achieve the lowest energy configuration using conjugate gradient algorithm. To prevent the interaction between the periodic images in the calculations, a vacuum layer with a thickness of approximately 25 Å is added along the z-direction (perpendicular to the monolayer) in the supercell. Note that a rectangular cell (see Figure 1) is used instead of primitive hexagonal one for applying strain along the desired direction. This is a commonly used approach[5, 17]. Geometry optimization is carried out employing the conjugated gradient technique and the convergence for the total energy is set as 10^{-7} eV. The Brillouin zone integration is sampled using a regular $6 \times 8 \times 1$ Monkhorst–Pack k-point grid, for geometry optimizations, while a denser grid of $12 \times 16 \times 1$ is used for density functional perturbation theory (DFPT) calculations. The elastic stiffness coefficients (C_{ij}) are obtained using a finite difference method as implemented in the VASP code. DFPT is used to calculate Born effective charges (Z_{ij}) and ionic and electronic parts of piezoelectric (e_{ij}) tensors.

III. RESULTS AND DISCUSSION

Table 1 shows the lattice parameters of the monolayers. We use a rectangular unit cell and lattice parameter a should be equal to $b\sqrt{3}$ for an ideal 1H structure. Our calculated lattice parameters are in good agreement with previously reported values[5, 9–11, 17]. 1H-$LaBr_2$ has significantly larger lattice parameters, compared to these of other two monolayers – mainly because ionic radius of La (Br) is larger than that of Mo/V(S) according to database http://abulafia.mt.ic.ac.uk/shannon/ptable.php . However, we notice that strip antiferromagnetic (AFM) ordered structures (shown in Figure 1) deviate from the ideal relationship, shrinking along the zigzag (b–axis)

	a (Å)	b (Å)	ϑ^{FM}	ϑ^{AFM}
1H-MoS_2	5.522	3.188	–	–
1H-VS_2(FM)	5.504	3.178	84.372 °	–
1H-VS_2(AFM)	5.502	3.154	84.177 °	84.518 °
1H-$LaBr_2$(FM)	7.298	4.214	84.189 °	–
1H-$LaBr_2$(AFM)	7.344	4.189	83.624 °	84.556 °

Table I. Structural information of the monolayers: optimized lattice parameters (a and b; see the rectangular cell in Fig 1) and the angle ∠Mo/V/La-S/Br-Mo/V/La. ϑ^{FM}(ϑ^{AFM}) is the angle ∠V↑/La↑-S/Br-V↑/La↑ (∠V↑/La↑-S/Br-V↓/La↓), where ↑ or ↓ arrows represent up or down spin polarization. The angle ∠Mo-S-Mo is 82.537 ° .

direction and expending along the armchair ($a-$axis) direction. We quantify this deviation as $(\frac{a-b\sqrt{3}}{b\sqrt{3}}) * 100\%$. This is about 1.22% (0.72%) for AFM 1H-$LaBr_2$ (1H-VS_2) monolayer. This deviation is also reflected in the change in angles ϑ^{FM} and ϑ^{AFM} (see Figure 1).

In agreement with previous reports[5, 9–11], we find that ferromagnetic (FM) ordering is the ground state for both 1H-$LaBr_2$ and 1H-VS_2 monolayers, lying 51.520 meV and 88.545 meV lower in energy compared to strip AFM state. However, the magnetic order of these monolayers has not been clearly identified in experiments to date. Although VS_2 monolayer has not yet been synthesized , ferromagnetism has been recently found in its ultra-thin films[21, 22].

1H-$LaBr_2$(FM) and 1H-VS_2(FM) monolayers belong to non-magnetic (i.e., just considering their structure but without considering their magnetic order) space group P6m2 (157), the same as 1H-MoS_2. This structure has no inversion symmetry and is intrinsically piezoelectric. We calculated their piezoelectric stress coefficients which are shown in Table 2. The piezoelectric coefficients that involve strain along z-direction are ill-defined for the monolayers. Our 1H monolayers have only one independent piezoelectric coefficient e_{11} (note that $e_{11} = -e_{12}$) due to $\bar{6}m2$ point group symmetry. Table 2 shows that 1H-MoS_2 has quite large e_{11}, compared to that of other two monolayers. Interestingly, 1H-$LaBr_2$(FM) shows a negative e_{11} which is also quite low compared to other materials. To understand the origin of piezoelectric constant, e_{11} *and* e_{12} can be decomposed into two parts[7, 23]:

$$e_{11} = e_{11}^{elc} + \sum_k e_{11}^{ion}(k) = e_{11}^{elc} + \sum_k \frac{ea}{A} Z_{11}(k) \frac{du_1(k)}{d\eta_1} \quad (1)$$

$$e_{12} = e_{12}^{elc} + \sum_k e_{12}^{ion}(k) = e_{12}^{elc} + \sum_k \frac{ea}{A} Z_{11}(k) \frac{du_1(k)}{d\eta_2} \quad (2)$$

The clamped-ion term (e_{11}^{elc} or e_{12}^{elc}) arises from the contributions of electrons when the ions are frozen at their zero-strain equilibrium internal atomic coordinates (u); and the internal-strain (e_{11}^{ion}) terms arises from the contribution from internal microscopic atomic displacements in response to a macroscopic strain. In our case, the strain (η_1) is applied in the x-direction (see Figure 1). Here, k runs over all the atoms in the unit cell, a is the in-plane lattice constant, e is the electron charge, and A is the area as 2D unit is used. The Born effective charge ($Z_{11}(k)$) of the k-th atom is calculated by the Berry-phase approach using DFPT. The response of the k-th atom's internal coordinate along the x-direction ($u_1(k)$) in response to a macroscopic strain (η_1) is measured by $\frac{du_1(k)}{d\eta_1}$. Table 2 shows that both e_{11}^{elc} and e_{11}^{ion} have same sign – positive – for 1H-MoS_2, unlike other two monolayers. This results in a large total $e_{11}$for 1H-MoS_2. Note that other 1H-MX_2 (M = Mo, W and X = S, Se, Te) monolayers also exhibit positive e_{11}^{elc} and e_{11}^{ion}[17]. However, due to the opposite sign of e_{11}^{elc} and e_{11}^{ion} in 1H-VS_2(FM), its total e_{11} is smaller than the e_{11} for 1H-MoS_2, even though it has a larger value of e_{11}^{elc} (see Table 2). Interestingly, 1H-$LaBr_2$(FM) shows a negative e_{11}^{ion} , which is significantly larger than its e_{11}^{elc}, thus resulting in a negative total e_{11}. This is different from recently discovered negative piezoelectric co-efficient in layered ferroelectricsthe and wurtzite, where negative sign comes from e_{11}^{elc}[6]. Here it is important to highlight that other 2D piezoelectrics – e.g., well-known h-BN monolayer[17] and 1H-VSe_2 monolayer[5] – have negative e_{11}^{ion}, but e_{11}^{elc} part dominates, resulting positive e_{11}.

Now to understand the origin of negative/positive e_{11}^{ion}, we expressed e_{11}^{ion} in terms of $Z_{11}$and $\frac{du_1(k)}{d\eta_1}$ (see eq.1). From Table 2, it is clear that the positive e_{11}^{ion} in 1H-MoS_2 is due to unusual BEC of Mo and S as we see a negative (positive) sign for cation Mo (anion S) in BEC. Such counter-intuitive BECs – Mo (S) shows a negative (positive) dynamical charge, opposite to its static positive charge –are also reported for bulk 2H-MoS_2[24]. Providing microscopic insight into the piezoelectric coefficients, BEC is – a dynamical charge – directly related to the change of electric polarization or dipole moment (for molecules) in response to an atomic displacement[25]. $Z_{11}(k)$ is proportional to $\frac{\partial P_1}{\partial \tau_1(k)}$, where ∂P_1 is the change of dipole moment in x-direction induced by a small displacement of atom k in the same direction ($\partial\tau_1(k)$)[25]. The negative slope ($\frac{\partial P_1}{\partial \tau_1(k)}$) will result a negative BEC, which is the case for 1H-MoS_2. This proportionality (i.e., the slope) is the origin of BECs and has the dimensionality of an electric charge. This charge is a well-defined and experimentally measurable quantity – owing to the fact that the BECs are related to the the LO–TO splitting, which is the frequency difference between the longitudinal (LO) and transverse (TO) optical phonon modes[25]. Compared to 1H-$LaBr_2$(FM), the magnitude of e_{11}^{ion} in 1H-$MoS_2$and 1H-VS_2(FM) is smaller because of smaller BECs and $\frac{du_1(k)}{d\eta_1}$. We find that large negative e_{11}^{ion} in 1H-$LaBr_2$(FM) originates from its large Z_{11} and $\frac{du_1(k)}{d\eta_1}$, both terms are almost two times larger than these of 1H-MoS_2or 1H-VS_2(FM). The large $\frac{du_1(k)}{d\eta_1}$ of 1H-$LaBr_2$(FM)

	e_{11}^{elc} (pC/m)	e_{11}^{ion}(pC/m)	e_{11}(pC/m)	Z_{11}(M)	Z_{11}(X)	$\frac{du_1}{d\eta_1}$(M)	$\frac{du_1}{d\eta_1}$(X)
1H-MoS_2	315.000	56.050	371.050	-1.006	0.503	-0.037	0.018
1H-VS_2(FM)	379.025	-80.925	298.100	1.359	-0.680	-0.038	0.021
1H-$LaBr_2$(FM)	111.175	-205.350	-94.175	2.540	-1.269	-0.069	0.035

Table II. The electronic (e_{11}^{elc}) and ionic (e_{11}^{ion}) part of the total piezoelectric stress constant e_{11} in 2D piezoelectric unit pC/m, born effective charge $Z_{11}$of M= Mo, V, and La and X= S and Br in $|e|$ unit, where e is the charge of an electron. Both 1H-$VS_2$and 1H-$LaBr_2$monolayers are in ferromagnetic (FM) state. $\frac{du_1}{d\eta_1}$ represents the change of the position of the atoms along a-direction under a strain along a-direction (η_1).

	C_{11}	C_{12}	ICOHP	ν	d_{11}
1H-MoS_2	133.214	33.105	-3.113	0.249	3.706
1H-VS_2(FM)	101.421	28.785	-2.510	0.284	4.104
1H-$LaBr_2$(FM)	30.338	9.534	-1.919	0.314	-4.527

Table III. Elastic constants (C_{11} and C_{12}) in N/m, the ICOHP of a bond between cation (Mo/V/La) and anion (S/Br) in eV/bond unit, the Poisson's ratio $\nu = C_{12}/C_{11}$ and piezoelectric strain coefficient in d_{11} pm/V.

can be due to its weaker La-Br bond (see Table 3) indicated by integrated crystal orbital Hamilton population (ICOHP). In addition, compared to other two monolayers, its larger lattice parameters (see Table 1) can promote larger displacement of atoms in response to strain as atoms have more space to move. We believe that BECs and lattice parameters – rather than static charges like Bader charge – can be ideal descriptors for searching better 2D piezoelectrics as they are directly related to the e_{ij}. Our results also explain previous observation that there is no significant correlation of d_{11} with electronegativity or Bader charges, whereas d_{11} shows a strong correlation with polarizatbilities of anions and cations[12]. Note that BECs can be considered as a manifestation of local polarizabilities of atoms[25].

Now we calculate the piezoelectric stress constants (d_{ij}) using e_{ij} and elastic constants (C_{ij}) (see Table 3). First, the mechanical/elastic stability of ferromagnetic (FM) 1H-$LaBr_2$ monolayer is checked according to the criteria for a 2D hexagonal crystal structure[26]: $C_{11} > C_{12}$ and $C_{66} > 0$. Considering the two independent elastic constants (only two independent elastic constants due to space group P6m2 and two-dimensionality) that we obtain, namely C_{11}= 30.34 N/m, C_{12}= 9.53 N/m, (notice that $C_{66} = (C_{11} - C_{12})/2$) it can be concluded that the monolayer is mechanically stable. The dynamic stability of 1H-$LaBr_2$ in terms of phonon modes has already predicted[9]. Our calculated elastic coefficients for the monolayers are in good agreement with the previously reported values[5, 9, 17]. Compared to 1H-$MoS_2$and 1H-VS_2(FM) monolayers, its lower C_{11} and C_{12} but larger ν indicate that 1H-$LaBr_2$(FM) monolayer is much softer. This is also expected because of its larger lattice parameters. This softening of elastic coefficients can also be understood from bond strength analysis. For that, we use ICOHP approach[27], which mainly quantifies the strength of the covalency of a bond. The more negative ICOHP, the stronger the bonding. We see in Table 3 that 1H-$LaBr_2$(FM) monolayer has significantly weaker La-Br bond (bond length: 3.143Å), compared to that of Mo-S (2.417Å) or V-S (2.366Å) bond. Table 3 shows that d_{11}(again only independent coefficient due to symmetry and dimensionality; and $d_{11} = \frac{e_{11}}{C_{11}-C_{12}}$) of 1H-$LaBr_2$(FM) is about 22% larger than that of well-known 2D piezoelectric 1H-MoS_2 because former has quite low elastic constants. The origin of negative sign in $d_{11}$of 1H-$LaBr_2$(FM) is in its negative e_{11}, which is discussed above.

Now we discuss how the magnetic ordering can affect on the piezoelectric response. We consider simple strip-type antiferromagnetic (AFM) order (see Figure 1). The calculated e_{11} and e_{12} are shown in Table 4. Interestingly, we find that e_{11} is not equal to minus e_{12} for AFM, whereas $e_{11} = -e_{12}$ for FM. Moreover, e_{11} in AFM is quite different from e_{11} in FM (see Table 4) – for example, e_{11} of 1H-$LaBr_2$(AFM) is almost double compared to that of FM, however e_{11} is still negative. To understand the origin of $e_{11} \neq -e_{12}$ for AFM, we consider two cases: (i) the structures (lattice parameters a and b and atomic positions) are relaxed, and (ii) AFM order is used, keeping lattice parameters a and b and atomic positions are fixed in their FM structures, which are represented by * in Table 4. We see that it is the change in magnetic order that intrinsically causes $e_{11} \neq -e_{12}$ for AFM – not the structural changes associated to this magnetic order change, although the structural relaxation changes the values too. Both $e^{elc}$and e^{ion} change in response to change in magnetic order. Table 4 also shows how the BECs and $\frac{du(k)}{d\eta}$ change, resulting in changes to e^{ion}.

IV. CONCLUSION

We show that 1H-$LaBr_2$ monolayer exhibits unusual in-plane negative piezoelectric coefficient, unlike many other 1H structured 2D piezoelectrics[12–15]. Here the origin of negative piezoelectric coefficient is because of large negative e_{11}^{ion} that can not be compensated by e_{11}^{elc}; this is different from hitherto observed negative piezocoefficients in some bulk materials due to large e_{ij}^{elc}[6, 8]. 1H-$LaBr_2$ monolayer is a promising 2D piezoelectric,

	e_{11}^{elc}	e_{11}^{ion}	e_{11}	Z_{11}(M)	Z_{11}(X)	$\frac{du_1(M)}{d\eta_1}$	$\frac{du_1(X)}{d\eta_1}$	e_{12}^{elc}	e_{12}^{ion}	e_{12}	$\frac{du_1(M)}{d\eta_2}$	$\frac{du_1(X)}{d\eta_2}$
1H-VS_2	221.900	-38.375	183.525	0.662	-0.210	-0.031	0.015	-284.150	12.175	-271.975	0.025	-0.013
1H-VS_2*	218.075	-14.525	203.550	0.657	-0.203	-0.033	0.016	-280.825	40.200	-240.625	0.026	-0.013
1H-$LaBr_2$	43.650	-269.025	-225.375	2.765	-1.381	-0.079	0.040	-96.225	199.300	103.075	0.066	-0.033
1H-$LaBr_2$*	57.275	-281.000	-223.725	2.744	-1.370	-0.083	0.041	-100.075	197.700	97.625	0.068	-0.034

Table IV. The electronic (e_{11}^{elc} and e_{12}^{elc}) and ionic (e_{11}^{ion} and e_{12}^{ion}) part of the total piezoelectric stress constant $e_{11}$and e_{12} of antiferromagnetic 1H-$VS_2$and 1H-$LaBr_2$ monolayer in 2D piezoelectric unit pC/m, born effective charge $Z_{11}$of M= Mo, V, and La and X= S and Br in $|e|$ unit, where e is the charge of an electron. $\frac{du_1}{d\eta_2}$ represents the change of the position of the atoms along a-direction under a strain along b-direction (η_2). 1H-VS_2*(1H-$LaBr_2$*) represents antiferromagnetic 1H-VS_2(1H-$LaBr_2$) monolayer in its ferromagnetic structure (*i.e.,* just the magnetic order is changed, no structural relaxation).

having large piezoelectric d_{11}(-4.527 pm/V) coefficient, which is comparable to that of well-known 2D piezoelectric 1H-MoS_2or 1H-VS_2 monolayers, and is larger than that of bulk wurtzite GaN (d_{33} ~ 3.1 pm/V). We also explain the origin – both sign and magnitude – of the piezoelectric coefficients of three monolayers (1H-$LaBr_2$, 1H-$MoS_2$and 1H-VS_2 monolayers) in terms of their dynamical charges (BECs) and atomic sensitivity ($\frac{du}{d\eta}$) to an applied strain. Being directly linked with e_{ij}, we believe that BECs –rather than static charge like Bader charge – can be good parameters for searching new 2D piezoelectrics, also providing insight into the underlying mechanism. Additionally, we show that change in magnetic order can affect on their piezo-response quite significantly, which can be a unique way for coupling magnetism and electromechanical properties in 2D magnets.

[1] Zhang, Q.; Zuo, S.; Chen, P.; Pan, C. Piezotronics in two-dimensional materials. *InfoMat* **2021**, *3*, 987–1007.

[2] Liu, Y.; Wahyudin, E. T. N.; He, J.-H.; Zhai, J. Piezotronics and piezo-phototronics in two-dimensional materials. *MRS Bulletin* **2018**, *43*, 959â964.

[3] Schaibley, J. R.; Yu, H.; Clark, G.; Rivera, P.; Ross, J. S.; Seyler, K. L.; Yao, W.; Xu, X. Valleytronics in 2D materials. *Nature Reviews Materials* **2016**, *1*, 16055.

[4] Shahnazaryan, V.; Rostami, H. Nonlinear exciton drift in piezoelectric two-dimensional materials. *Phys. Rev. B* **2021**, *104*, 085405.

[5] Yang, J.; Wang, A.; Zhang, S.; Liu, J.; Zhong, Z.; Chen, L. Coexistence of piezoelectricity and magnetism in two-dimensional vanadium dichalcogenides. *Phys. Chem. Chem. Phys.* **2019**, *21*, 132–136.

[6] Qi, Y.; Rappe, A. M. Widespread Negative Longitudinal Piezoelectric Responses in Ferroelectric Crystals with Layered Structures. *Phys. Rev. Lett.* **2021**, *126*, 217601.

[7] Noor-A-Alam, M.; Z. Olszewski, O.; Nolan, M. Ferroelectricity and Large Piezoelectric Response of AlN/ScN Superlattice. *ACS Applied Materials & Interfaces* **2019**, *11*, 20482–20490.

[8] Liu, S.; Cohen, R. E. Origin of Negative Longitudinal Piezoelectric Effect. *Phys. Rev. Lett.* **2017**, *119*, 207601.

[9] Zhao, P.; Ma, Y.; Lei, C.; Wang, H.; Huang, B.; Dai, Y. Single-layer LaBr2: Two-dimensional valleytronic semiconductor with spontaneous spin and valley polarizations. *Applied Physics Letters* **2019**, *115*, 261605.

[10] Badrtdinov, D. I.; Nikolaev, S. A. Localised magnetism in 2D electrides. *J. Mater. Chem. C* **2020**, *8*, 7858–7865.

[11] Jiang, Z.; Wang, P.; Xing, J.; Jiang, X.; Zhao, J. Screening and Design of Novel 2D Ferromagnetic Materials with High Curie Temperature above Room Temperature. *ACS Applied Materials & Interfaces* **2018**, *10*, 39032–39039.

[12] Blonsky, M. N.; Zhuang, H. L.; Singh, A. K.; Hennig, R. G. Ab Initio Prediction of Piezoelectricity in Two-Dimensional Materials. *ACS Nano* **2015**, *9*, 9885–9891.

[13] Michel, K. H.; Çakır, D.; Sevik, C.; Peeters, F. M. Piezoelectricity in two-dimensional materials: Comparative study between lattice dynamics and ab initio calculations. *Phys. Rev. B* **2017**, *95*, 125415.

[14] Alyrk, M. M.; Aierken, Y.; Çakır, D.; Peeters, F. M.; Sevik, C. Promising Piezoelectric Performance of Single Layer Transition-Metal Dichalcogenides and Dioxides. *The Journal of Physical Chemistry C* **2015**, *119*, 23231–23237.

[15] Lu, Y.; Sinnott, S. B. Density Functional Theory Study of Epitaxially Strained Monolayer Transition Metal Chalcogenides for Piezoelectricity Generation. *ACS Applied Nano Materials* **2020**, *3*, 384–390.

[16] Zhu, H.; Wang, Y.; Xiao, J.; Liu, M.; Xiong, S.; Wong, Z. J.; Ye, Z.; Ye, Y.; Yin, X.; Zhang, X. Observation of piezoelectricity in free-standing monolayer MoS2. *Nature Nanotechnology* **2015**, *10*, 151–155.

[17] Duerloo, K.-A. N.; Ong, M. T.; Reed, E. J. Intrinsic Piezoelectricity in Two-Dimensional Materials. *The Journal of Physical Chemistry Letters* **2012**, *3*, 2871–2876.

[18] Perdew, J. P.; Burke, K.; Ernzerhof, M. Generalized Gradient Approximation Made Simple. *Phys. Rev. Lett.* **1996**, *77*, 3865.

[19] Kresse, G.; Furthmüller, J. Efficient iterative schemes for ab initio total-energy calculations using a plane-wave basis set. *Phys. Rev. B* **1996**, *54*, 11169.

[20] Kresse, G.; Joubert, D. From ultrasoft pseudopotentials to the projector augmented-wave method. *Phys. Rev. B* **1999**, *59*, 1758.

[21] Gao, D.; Xue, Q.; Mao, X.; Wang, W.; Xu, Q.; Xue, D. Ferromagnetism in ultrathin VS2 nanosheets. *J. Mater. Chem. C* **2013**, *1*, 5909–5916.

[22] Zhong, M.; Li, Y.; Xia, Q.; Meng, X.; Wu, F.; Li, J. Ferromagnetism in VS2 nanostructures: Nanoflowers versus ultrathin nanosheets. *Materials Letters* **2014**, *124*, 282–

285.

[23] Bernardini, F.; Fiorentini, V.; Vanderbilt, D. Spontaneous polarization and piezoelectric constants of $III-V$ nitrides. *Phys. Rev. B* **1997**, *56*, R10024–R10027.

[24] Pike, N. A.; Van Troeye, B.; Dewandre, A.; Petretto, G.; Gonze, X.; Rignanese, G.-M.; Verstraete, M. J. Origin of the counterintuitive dynamic charge in the transition metal dichalcogenides. *Phys. Rev. B* **2017**, *95*, 201106.

[25] Ghosez, P.; Michenaud, J.-P.; Gonze, X. Dynamical atomic charges: The case of ABO_3 compounds. *Phys. Rev. B* **1998**, *58*, 6224–6240.

[26] Mouhat, F.; Coudert, F.-X. Necessary and sufficient elastic stability conditions in various crystal systems. *Phys. Rev. B* **2014**, *90*, 224104.

[27] Maintz, S.; Deringer, V. L.; Tchougréeff, A. L.; Dronskowski, R. LOBSTER: A tool to extract chemical bonding from plane-wave based DFT. *Journal of Computational Chemistry* **2016**, *37*, 1030–1035.